Exergetic, economic and environmental analyses and multi-objective optimization of an SOFC-gas turbine hybrid cycle coupled with an MSF desalination system

Behzad Najafi [a], Ali Shirazi [b,*], Mehdi Aminyavari [c], Fabio Rinaldi [a], Robert A. Taylor [b]

[a] Dipartimento di Energia, Politecnico di Milano, Via Lambruschini 4, 20156 Milano, Italy
[b] School of Mechanical and Manufacturing Engineering, The University of New South Wales (UNSW), Kensington, New South Wales 2052, Australia
[c] Scuola di Ingegneria Industriale, Campus di Piacenza, Politecnico di Milano, Via Scalabrini, 76, 29100 Piacenza, Italy

Article history:
Received 26 September 2013
Received in revised form 28 November 2013
Accepted 30 November 2013
Available online 22 December 2013

1. Introduction

According to the U.S. energy information administration (EIA), the electrical energy demand is expected to rise by 22% from current levels by 2035 [1]. If this growth is met by conventional technology, it could create negative environmental ramifications. At the same time, increasing demand for rapidly diminishing fresh water resources has become a global challenge [2]. Cogeneration is defined as the combined production of electricity with other useful forms of energy. By getting more from the same primary energy source, cogeneration results in higher exergetic efficiency, lower pollutant emissions, and lower operational and maintenance costs [3,4].

Fuel cell systems are interesting alternatives (albeit commercially underdeveloped) to conventional power generation systems owing to their high efficiency and low emissions [5]. Among the various types of fuel cells available, solid oxide fuel cells (SOFCs) are key candidates for integration with gas turbines (GTs), owing to their high operating temperature (between 600 °C and 1000 °C). The resulting hybrid SOFC–GT system is a highly efficient power generation unit with the overall electrical conversion efficiency approaching 65% [6]. Adding a heat recovery exchanger also facilitates the possibility of integration of this unit with other thermal systems [7–11]. Accordingly, numerous studies have been carried out on modeling of hybrid SOFC cycles [12–15].

Potable water production is a major untapped application of these hybrid systems—particularly in areas (like the Middle East) which are

* Corresponding author. Tel.: +61 413077896.
E-mail addresses: behzad.najafi@polimi.it (B. Najafi), a.shirazi@student.unsw.edu.au (A. Shirazi), mehdi.aminyavari@mail.polimi.it (M. Aminyavari), fabio.rinaldi@polimi.it (F. Rinaldi), Robert.Taylor@unsw.edu.au (R.A. Taylor).

Nomenclature

A	area (m^2)
c_{elec}	electricity unit cost (USD/kWh)
c_f	fuel unit cost (USD/MJ)
c_p	specific heat at constant pressure (kJ/kg K)
CRF	capital recovery factor
c_w	distillate product unit cost (USD/m^3)
$\dot{C}_{env}$	social cost of air pollution (USD/s)
$\dot{C}_{tot}$	total cost rate (USD/s)
e	specific exergy (kJ/kg)
$\dot{E}$	exergy flow rate (kW)
$\bar{e}$	specific exergy (kJ/kmol)
h	specific enthalpy (kJ/kg)
H_b	brine pool height (m)
i	current density (A/m^2), interest rate (%)
k	specific heat ratio
LHV	low heating value (kJ/kg)
$\dot{m}$	mass flow rate (kg/s)
N	operational hours in a year
n	number of desalination stages, system life time (year)
p	pressure (kpa, bar), payback period (year)
PR	thermal performance ratio
$\dot{Q}$	the time rate of heat transfer (kW)
$\bar{R}$	Universal gas constant (kJ/kmol K)
r_p	pressure ratio
s	specific entropy (kJ/kg K)
S/C	steam to carbon ratio
T	temperature (K or °C)
TBT	top brine temperature (°C)
TIT	turbine inlet temperature (K)
T_n	brine temperature in the last stage (°C)
T_s	inlet motive steam temperature (°C)
TTD	terminal temperature difference (°C)
U	overall heat transfer coefficient (kW/m^2 K)
U_a	air utilization factor
U_f	fuel utilization factor
V	voltage (V)
V_v	vapor velocity (m/s)
$\dot{W}$	mechanical work (kW)
X	salt concentration (ppm)
x	molar fraction
X_b	blow-down brine salt concentration (ppm)
X_f	intake seawater salt concentration (ppm)
X_r	recycle brine salt concentration (ppm)
Z	capital cost (USD)
$\dot{Z}$	capital cost rate (USD/s)

Greek symbols

η	efficiency
λ	specific latent heat (kJ/kg)
ρ	density (kg/m^3)
Φ	maintenance factor
ψ	exergetic efficiency

Subscripts

AC	air compressor
ap	approach point
aux	auxiliary
b	brine
BH	brine heater
C	condenser
CC	combustion chamber
CH	chemical
cv	control volume
cw	cooling water
D	destruction
d	distillate product
dc	discharge
ec	economizer
ev	evaporator
f	fuel
FC	fuel compressor
G	electric generator
g	gas
GT	gas turbine
HR	heat recovery
HRSG	heat recovery steam generator
HJ	heat rejection
i	inlet
LMTD	Logarithmic Mean Temperature Difference
MSF	multi stage flash
o	outlet
PH	physical
pp	pinch point
PT	power turbine
REC	recuperator
s	steam
st	stage
suc	suction
sw	seawater
T	turbine
t	tube
tot	total
v	vapor
w	water

facing water scarcity. Since desalination is relatively expensive and requires considerable energy input, cogeneration represents a promising way to lower these barriers to technological uptake [16]. Thermal desalination systems, such as multi stage flash distillation (MSF) and the multi effect distillation (MED), can potentially be coupled with heat recovery steam generators for integration with thermal power plants [17]. Of the two, MSF is a more commonly used desalination technology due to its simple layout and reliable performance. This is especially true in the Middle East where the temperature, salt content, biological activity, and pollution level of the raw water are all relatively high [18].

Accordingly, we propose that for these climates an SOFC–GT plant integrated with an MSF desalination unit can be an appropriate design configuration. To accomplish this, a heat recovery steam generator (HRSG) is utilized to recover the heat wasted from the SOFC–GT system to produce the required motive saturated steam for the MSF unit.

A limited number of studies have investigated the feasibility of integrating fuel cells and desalination units in the past ten years. Hallaj et al. [19], in a conceptual study, demonstrated that the fuel cell based combined heat and power (CHP) systems can be efficiently integrated with reverse osmosis (RO) and MSF desalination units. Their configuration utilized a dual-purpose plant consisting of a molten carbonate fuel cell integrated with an MSF desalination plant. This plant design showed an improvement of 5.61% in global system efficiency. Lisbona et al. [20] investigated different configurations of fuel cell systems integrated with RO and MSF desalination units from energetic and economic viewpoints. In their estimated future scenario, the recovery period of the hybrid RO systems integrated with both MCFC and SOFC was found to be 9 years.

Several studies have also been dedicated to energetic analysis of integrated systems composed of desalination units and conventional power generation systems. These include humidification–dehumidification

desalination unit integrated with a gas turbine [21], MSF and MED desalination systems coupled to gas and steam turbines [16,22–24], and desalination units integrated with combined cooling, heating and power (CCHP) systems [25–27].

In the preceding studies, only first law analysis was employed to investigate the performance of the plant. Exergy analysis, based on both the first and second laws, is more informative since it serves to identify the source and magnitude of thermodynamic inefficiencies in a given process [28]. Hosseini et al. [29] proposed an SOFC and micro GT system integrated with an MED unit and modeled the proposed system based on both energy and exergy analyses. The results showed that fuel cell stack pressure has a significant influence on the integrated system capacity and also increases the system energy efficiency. Several studies have also carried out exergy analyses of SOFC–GT cycles and different desalination technologies. Akkaya et al. [13] developed a thermodynamic model of an SOFC–GT CHP plant and analyzed the exergetic performance of the system to obtain a more efficient design by the determining thermodynamic irreversibilities. The results revealed that a design based on the maximum exergetic performance coefficient (EPC) has the lowest entropy generation rate for a given total exergy output. Wang et al. [14] proposed a new integrated power generation system driven by an SOFC unit using the Kalina cycle to recover the waste heat of exhaust from the SOFC–GT cycle. In their study, an exergy analysis was conducted to identify the sources of thermodynamic inefficiencies in each system component. The results demonstrated that the largest exergy destruction occurs in the SOFC unit followed by the afterburner, the waste heat boiler, and the gas turbine. Kahraman and Cengel [30] developed a thermodynamic model of a large MSF desalination plant and analyzed the system from an exergy standpoint. The results showed that the highest exergy destruction rate occurs in the MSF unit, and the second law efficiency of the system was 4.2%. Al-Weshahi et al. [31] carried out a similar study on a 3800 m^3/h MSF desalination plant and concluded that the exergetic efficiency of the system can be improved from 5.8% to 14% by recovering the hot distillate water from heat recovery stages.

Economic considerations should also be taken into account as this determines whether or not it makes sense to actually build a cogeneration plant. Thus, the thermodynamics and economics are inexorably linked and proposed systems must be considered from both points of view. Only a few studies have approached SOFC–GT systems with this framework. Cheddie conducted a thermo-economic analysis of an indirectly coupled SOFC–GT system [32]. In their work, the SOFC stack was proposed to be coupled with an existing GT power plant at full load operating conditions to improve the system performance. The results revealed that the second law efficiency of the system can be improved from 28.9% for the standard plant to 46.7% for the hybrid system, while the electricity generation cost can be reduced from 5.46 to 4.54¢ kWh^{-1} as a result of the coupling. Moreover, a thermo-economic analysis of a combined power and MSF desalination plant was presented by Hosseini et al. [33]. The economic model of the system was developed based on the Total Revenue Requirement (TRR) method and the obtained levelized costs (including capital, maintenance, and operational costs) were used as input data for thermo-economic analysis of the system. They obtained a total exergetic efficiency of 27% and total capital cost of $115,696,000 while the cost rate of water production was determined to be 1.886 $ m^{-3}. Ansari et al. [34] performed a thermo-economic optimization of a pressurized water reactor power plant coupled to an MED desalination system with thermo-vapor compressor (TVC) for simultaneous production of power and fresh water. The cost of the system product (including the cost of generated electricity and fresh water) was defined as objective function and minimized through genetic algorithm. The results obtained from thermo-economic optimization showed that the capital investment, the cost of exergy destruction, the cost of electric power generation and the cost of fresh water production were respectively reduced by 4.4%, 0.5%, 13.4% and 27.5% compared to the base case system.

The multi-objective optimization method is an efficient approach for dealing with conflicting objectives (e.g. cost vs. efficiency) [35,36]. A multi-objective thermo-economic optimization of an SOFC–GT hybrid system was conducted by Autissier et al. [37] in which different optimal designs with costs from 2400 $ kW^{-1} to 6700 $ kW^{-1} (leading to 44% and 70% efficiency, respectively) were obtained. A similar study on a planar SOFC system was also carried out by Palazzi et al.—optimal designs were found with efficiencies ranging from 34% to 44% [38].

Besides the thermal efficiency and the cost of the power generation system, emission effects of these plants have also been taken into account in the recent studies. Sayyadi et al. [39] conducted a multi-objective exergoeconomic and environmental optimization on a benchmark cogeneration plant and obtained a Pareto front with cost rates ranging from 0.83 to 2.7 $\$s^{-1}$ and exergetic efficiencies ranging from 48% to 55%. Raluy et al. [40] analyzed the environmental impacts of various commercially available desalination technologies integrated with different energy production systems. The results revealed that the environmental load of MSF and MED desalination technologies can be brought down by 75% when they are properly coupled with hybrid plant based on a combined cycle. In previous paper of the co-authors [41], a multi-objective optimization was applied to an SOFC–GT system where the total cost rate of system, including the social cost of emissions, was considered for a fully optimized system.

Furthermore, a similar approach has also been utilized in recent multi-objective optimization of desalination systems integrated with conventional power generation systems. Hosseini et al. [42] conducted a multi-objective optimization on a combined GT and MSF desalination plant in which a thermo-environmental objective function and the total exergetic efficiency of the system were taken into account as optimization objectives. The results showed that the cost of products and environmental cost impact are reduced by 13.4% and 53.4% respectively, while a 14.8% rise is obtained in total exergetic efficiency. Sanaye and Asgari [43] also employed a similar method to optimize combined cycle power plants integrated with an MSF desalination unit. Their study resulted in a Pareto front with designs leading to total an exergy destruction ranging from 465 to 484 MWs, while requiring total annual costs of 192 to 214 million USD per year.

To the authors' knowledge, no thorough exergetic and economic study has been conducted on an integrated SOFC–GT–MSF system thus far. Furthermore, the above literature summary reveals that the published literature rarely includes an environmental (emissions cost) analysis as part of a multi-objective optimization.

Motivated by this research gap, the present work presents thermal (energy and exergy), economic, and environmental (emissions cost) analyses as well as multi-objective optimization for an IRSOFC–GT hybrid power generation system coupled to an MSF desalination plant with brine recirculation. First, the whole system is modeled analytically and then the multi-objective optimization is performed to achieve optimal design parameters. The considered objective functions are the exergetic efficiency (to be maximized) and the total cost rate (to be minimized). The later includes the capital and maintenance cost of the plant, the fuel cost and cost of the environmental impact. Finally, the payback period of the system is evaluated to determine the required time for recovering the investment cost of the plant.

2. System description

A promising alternative for utilizing the waste heat generated by high temperature fuel cells is integrating these units with thermal desalination systems [19]. Accordingly, a logical configuration for such a hybrid system is to produce steam in a heat recovery steam generator by utilizing the waste heat of the flue gases from the SOFC–GT system; the steam which is subsequently utilized in the MSF desalination unit. Fig. 1 illustrates the schematic diagram of an integrated SOFC–GT–MSF system for simultaneous generation of the electricity and fresh water.

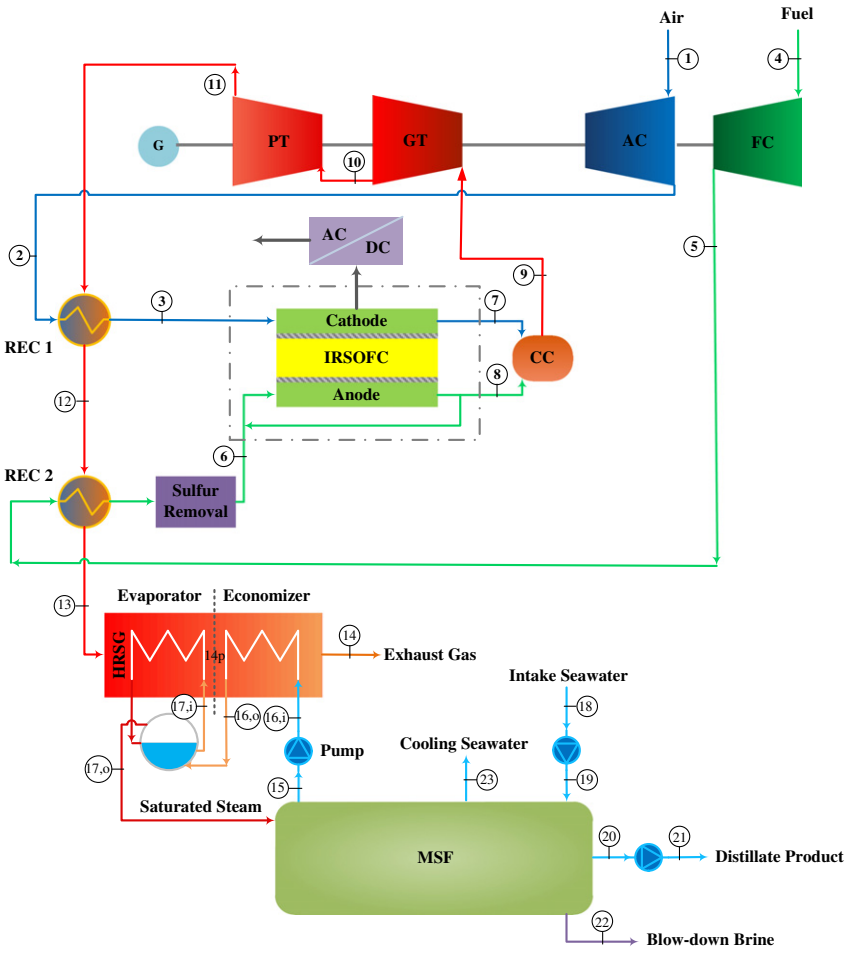

Fig. 1. Schematic diagram of IRSOFC–GT hybrid cycle coupled to MSF desalination system with brine recirculation.

The power generation cycle (which is fed by natural gas) consists of an air compressor (AC), a fuel compressor (FC), an internal reforming solid oxide fuel cell (IRSOFC) stack, a DC/AC inverter, air and fuel recuperators (REC1 and REC2), a combustion chamber (CC), gas and power turbines (GT and PT), an electric generator (G), and a heat recovery steam generator (HRSG).

The following is a brief description of power generation cycle flow diagram shown in Fig. 1: The ambient air enters the cycle at node 1, is compressed by the air compressor (AC) up to node 2, and then is heated in the air recuperator (REC1), reaching node 3, after which it enters the cathode compartment of the SOFC stack. Similarly, natural gas entering the plant at node 4 is compressed by the fuel compressor (FC), is preheated in the corresponding recuperator (REC2), and afterwards proceeds to the desulphurization unit. The sulfur free fuel (node 6), after being mixed with the anode recirculation stream, enters the anode compartment of the stack together with the required steam. The resulting mixed stream undergoes the reforming process leading to hydrogen-rich products which participate in the electrochemical reaction taking place within the fuel cell stack. ADC to AC inverter converts the DC power generated by the stack into grid quality electricity. The electrochemical reaction taking place inside the SOFC stack also generates thermal energy. A part of this is used to provide the required heat of the internal reforming reaction, another part is employed to heat up the cell products and residual reactants, and the remaining amount is transferred to the environment as a heat loss. High temperature streams of air leave on the cathode side (node 7). Exhausted fuel, which is the non-reacted part of the reformed natural gas, exits on the anode side (node 8) and then enters the combustion chamber in which the remaining fuel is burnt with excess air. The resulting flue gas (node 9) goes through the gas turbine (GT) which provides the required power of the fuel and air compressors. The flue gas subsequently expands through the power turbine (PT)—generating additional useful work which leads to further electrical power production. Flue gas leaving the power turbine (node 11) goes through the air and fuel recuperators. The remaining thermal energy left over at node 13 is utilized in the heat recovery steam generator (HRSG) to produce the required saturated steam of the distillation unit. Eventually, the exhaust gas is discharged to the atmosphere at node 14.

The MSF desalination portion of the system (with brine recirculation) is also schematically illustrated in Fig. 2. This cycle includes three main sections: the heat input section (brine heater), the heat recovery section (HR), and the heat rejection section (HJ). The recovery and rejection sections both have a series of stages. Each stage has a flash chamber and a condenser where the vapor is flashed off in the chamber and later condensed. The flash chamber is separated from the condenser by a demister, where entrained brine droplets are removed from the flashing vapor.

The main principles of this type of desalination system operation can be summarized as follows: The intake seawater flows ($\dot{m}_f + \dot{m}_{cw}$) through the condenser tubes of the heat rejection section where its temperature increases to a higher temperature by gaining the latent heat of the condensing fresh water vapor. At the output of the first rejection stage, the warm stream of intake seawater splits into two parts: the cooling seawater stream ($\dot{m}_{cw}$), which is rejected back to the sea and the feed seawater stream ($\dot{m}_f$), which is mixed in the brine pool of the last flashing stage in the heat rejection section. The function of the cooling seawater is to remove the excess heat added to the system by the saturated motive steam in the brine heater. In the last stage of the

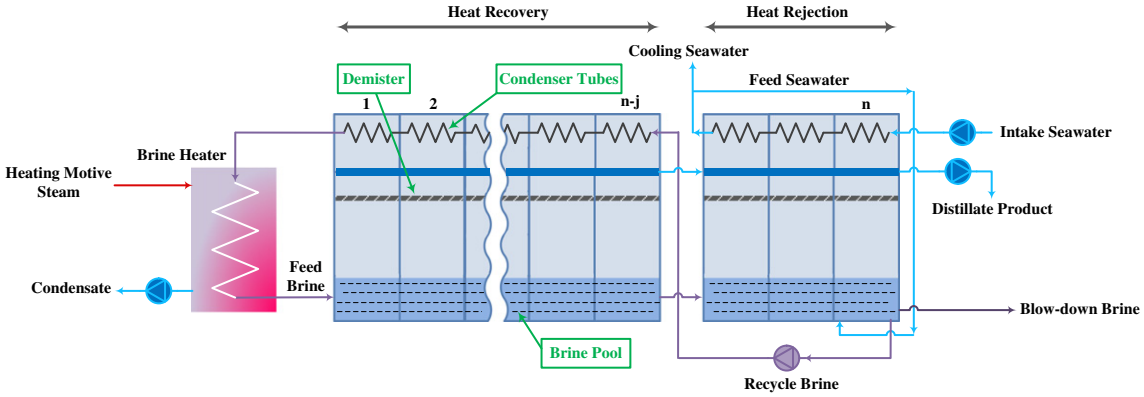

Fig. 2. Schematic diagram of an MSF desalination system with brine recirculation.

heat rejection section, two flows are extracted from the brine pool, which includes the blow-down brine and the recycle brine. The blow-down brine flow ($\dot{m}_b$) is rejected to the sea, which controls the salt concentration of the cycle. The recycle brine stream ($\dot{m}_r$) then enters the condenser tubes of the last stage of the heat recovery section where its temperature increases as it flows in the condenser tubes across the stages by absorbing the latent heat of the condensing fresh water vapor in each stage. Subsequently, the recycle brine stream passes through the brine heater tubes where motive saturated steam ($\dot{m}_s$) is condensed on the outside surface of the tubes. This step increases the temperature of the recycle brine to the desired value known as the top brine temperature (TBT). The hot brine enters the flashing stages where a small amount of fresh water vapor is formed by brine flashing in each stage. This vapor passes through the demister and is condensed onto the heat exchanger where the cold recycle brine flow passes through and recovers the latent heat of the fresh water vapor. Finally, the condensed vapor drips onto a distillate tray and is accumulated across the stages as the desired distillate product.

3. System analysis

Thermodynamic modeling of the aforementioned cogeneration system is presented here on the basis of thermal (energy and exergy), economic, and environmental analyses. This section describes these individually by discussing the salient assumptions and components for each category.

3.1. Energy analysis

To simplify the analysis procedure, the following assumptions have been employed while developing the cogeneration system model:

- All gases are treated as ideal gases and gas leakage is negligible.
- All the system components operate under steady state conditions.
- Internal distribution of temperature, pressure, and gas compositions in each component is uniform.
- Cathode and anode temperatures are assumed to be the same.
- Changes in the kinetic and potential energies of fluid streams are negligible.
- All system components, except for fuel cell stack and combustion chamber, are adiabatic.
- The fuel supplied to the system is assumed to be natural gas.
- Subcooling of condensate or superheating of heating motive steam is negligible in the brine heater.
- Equal flashing and recycle brine temperature changes per stage are considered.
- In the heat rejection section, the feed seawater is heated to a temperature equal to the brine temperature in the last flashing stage.
- The salt concentration of the intake seawater is constant and the distillate product is salt free.
- The seawater is an ideal mixture of two components (salt and water—free of sand, dirt, and biomass).
- Due to environmental issues, the maximum salt concentration of the blow-down brine is 70,000 ppm.

Using these assumptions throughout our analysis, each system component and the corresponding equations can now be developed, as follows. In this work, MATLAB is used to develop the mathematical model of the whole system.

3.1.1. The solid oxide fuel cell–gas turbine cycle

The SOFC model developed in the present work is based on a tubular design, and the geometric and performance data are obtained from Refs. [44,45]. In an SOFC, DC power is generated via electrochemical reactions. Natural gas is reformed inside the anode compartment, producing hydrogen which is oxidized in the SOFC. The basic electrochemical reactions simultaneously occurring inside the SOFC stack are given by:

$$CH_4 + H_2O \rightarrow CO + 3H_2 \quad \text{(Reforming)} \tag{1}$$

$$CO + H_2O \rightarrow CO_2 + H_2 \quad \text{(Shifting)} \tag{2}$$

$$H_2 + \frac{1}{2}O_2 \rightarrow H_2O \quad \text{(Electrochemical)} \tag{3}$$

Eq. (1) is the methane reforming reaction where methane is reformed to hydrogen and carbon monoxide. Eq. (2) is the water–gas shifting reaction in which the produced carbon monoxide reacts with water to generate additional hydrogen and carbon dioxide. The methane reforming and water–gas shift reactions are considered to be at equilibrium. Finally, the third reaction results in the generation of electricity and water in the SOFC stack. The net chemical reaction inside the cell can be written as:

$$CH_4 + 2O_2 \rightarrow CO_2 + 2H_2O \tag{4}$$

Details of the governing equations for the thermodynamic model of the SOFC–GT system components (including compressors, SOFC stack, combustion chamber, gas turbine, power turbine, recuperators, and the water pump) were described in details in our previous paper [41].

3.1.2. Heat recovery steam generation

In order to integrate the MSF desalination system with the SOFC–GT cycle, a heat recovery steam generator (HSRG) is required to recover any remaining thermal energy of the high temperature exhaust gases at node 13 and provide the required motive steam for the MSF desalination system. The HRSG of the present work includes an economizer and an evaporator. It should be noted that since the required motive steam

is assumed to be saturated, a superheater section for the HRSG is not needed.

The temperature difference between water leaving the economizer ($T_{16,o}$) and the saturation temperature (T_s) is called the approach point, and is calculated by:

$$\Delta T_{ap} = T_s - T_{16,o} \tag{5}$$

The pinch point is defined as the minimum difference between the temperature of the gas at the evaporator entry and the saturation temperature, which can be obtained as follows:

$$\Delta T_{pp} = T_{14p} - T_{17,i} \tag{6}$$

The energy balance equation for the economizer, the evaporator, and the HRSG can be expressed as follows:

$$\dot{Q}_{ec} = \dot{m}_g\left(h_{14p} - h_{14}\right) = \dot{m}_s\left(h_{16,o} - h_{16,i}\right) \tag{7}$$

$$\dot{Q}_{ev} = \dot{m}_g\left(h_{13} - h_{14p}\right) = \dot{m}_s\left(h_{17,o} - h_{17,i}\right) \tag{8}$$

$$\dot{Q}_{HRSG} = \dot{m}_g(h_{13} - h_{14}) = \dot{m}_s\left(h_{17,o} - h_{16,i}\right) \tag{9}$$

3.1.3. MSF desalination with brine recirculation

Based on an energy analysis, the governing equations for thermodynamic modeling of the MSF desalination system derived from Ref. [18] are presented in this section.

The overall mass and salt balance equations for the MSF cycle are written as:

$$\dot{m}_f = \dot{m}_d + \dot{m}_b \tag{10}$$

$$X_f \dot{m}_f = X_b \dot{m}_b \tag{11}$$

where the terms $\dot{m}_f, \dot{m}_d$, and $\dot{m}_b$ are the corresponding mass flow rates of feed seawater, distillate product, and blow-down brine respectively, while X indicates the salt concentration.

The combination of Eqs. (10) and (11) can express the total feed seawater flow rate in terms of the distillate product mass flow rate, which is written as:

$$\dot{m}_f = \frac{X_b}{X_b - X_f}\dot{m}_d \tag{12}$$

The flashing brine temperature drop per stage (ΔT_{st}) is obtained as follows:

$$\Delta T_{st} = \frac{TBT - T_n}{n} \tag{13}$$

where TBT is top brine temperature, T_n is brine temperature in the last stage, and n is the number of desalination stages (HR and HJ stages).

The general expression for the flashing brine temperature in ith stage (T_i) is given by:

$$T_i = TBT - i\Delta T_{st} \quad i = 1, 2, \ldots, n \tag{14}$$

Also, the general equation for the recycle brine temperature leaving the condenser of the ith stage ($T_{r,i}$) is calculated as follows:

$$T_{r,i} = T_n + (n-j)\Delta T_r - (i-1)\Delta T_r \tag{15}$$

where j and ΔT_r are the number of heat rejection stages and the recycle brine temperature increase per stage, respectively.

The seawater temperature increase per stage in the heat rejection section (ΔT_j) is calculated by:

$$\Delta T_j = \frac{T_n - T_{sw}}{j} \tag{16}$$

where T_{sw} is the intake seawater temperature. Having ΔT_j derived, the general relation for the intake seawater temperature leaving the condenser in ith stage of the heat rejection section (T_{ji}) is:

$$T_{ji} = T_{sw} + (n - i + 1)\Delta T_j \tag{17}$$

More details on derivation of Eqs. (15) and (17) can be found in [18].

The general formula for the mass flow rate of distillate product in the ith stage ($\dot{m}_{d,i}$) can be obtained as follows:

$$\dot{m}_{d,i} = \dot{m}_r y(1-y)^{i-1} \tag{18}$$

where $\dot{m}_r$ is the recycle brine mass flow rate, and y is the specific ratio of sensible and latent heats, which is calculated by:

$$y = \frac{c_{p,r}\Delta T_{st}}{\lambda_v} \tag{19}$$

where $c_{p,r}$ and λ_v are the specific heat at constant pressure of the flashing brine and the specific latent heat of the flashing vapor formed in each stage. Therefore, summing the values of $\dot{m}_{d,i}$ for all stages, the total mass flow rate of distillate product ($\dot{m}_d$) is obtained as follows:

$$\dot{m}_d = \sum_{i=1}^{n}\dot{m}_{d,i} = \dot{m}_r\left[1-(1-y)^n\right] \tag{20}$$

Applying the salt balance equation for the last flashing stage, the salt concentration of the recycle brine stream (X_r) is estimated as follows:

$$X_r = \left[\frac{\dot{m}_f X_f + \left(\dot{m}_r - \sum_{k=1}^{n-1}\dot{m}_{d,k}\right)X_{n-1} - \dot{m}_b X_b}{\dot{m}_r}\right] \tag{21}$$

In general, the salt concentration of the flashing brine flow leaving the ith stage (X_i) can be found by:

$$X_i = \left(\frac{\dot{m}_r - \sum_{k=1}^{i-1}\dot{m}_{d,i}}{\dot{m}_r - \sum_{k=1}^{i}\dot{m}_{d,i}}\right)X_{i-1} \tag{22}$$

Furthermore, writing the energy balance equation for the brine heater and the whole MSF desalination system, the mass flow rates of required motive steam ($\dot{m}_s$) and cooling seawater ($\dot{m}_{cw}$) are obtained as follows:

$$\dot{m}_s = \frac{\dot{m}_r c_{p,r}\left(TBT - T_{r,1}\right)}{\lambda_s} \tag{23}$$

$$\dot{m}_{cw} = \frac{\dot{m}_s\lambda_s - \dot{m}_f c_{p,f}(T_n - T_{sw})}{c_{p,cw}(T_n - T_{sw})} \tag{24}$$

where λ_s is the specific latent heat of the motive steam.

The heat transfer surface area of the brine heater (A_{HB}) is calculated by:

$$A_{BH} = \frac{\dot{m}_s \lambda_s}{U_{BH} \times \Delta T_{LMTD,BH}} \tag{25}$$

The heat transfer surface area of the condenser in each stage of the heat recovery section ($A_{HR,i}$) is computed as follows:

$$A_{HR,i} = \frac{\dot{m}_r c_{p,r,i}\left(T_{r,i} - T_{r,i+1}\right)}{U_{HR,i} \times \Delta T_{LMTD,HR,i}} \tag{26}$$

Similarly, the heat transfer surface area of the condenser in each stage of the heat rejection section ($A_{HJ,ji}$) is given by:

$$A_{HJ,ji} = \frac{(\dot{m}_f + \dot{m}_{cw}) c_{p,r,i}\left(T_{j,i} - T_{j,i+1}\right)}{U_{HJ,i} \times \Delta T_{LMTD,HJ,i}} \quad i = n - j + 1, \ldots, n \tag{27}$$

The terms U and ΔT_{LMTD} for the brine heater and the condenser of HR and HJ sections are determined by a set of comprehensive empirical equations presented in Ref. [18].

Thus, the specific heat transfer surface area of the MSF desalination system (sA_{MSF}) is defined as:

$$sA_{MSF} = \frac{A_{BH} + (n-j)A_{HR,i} + (j)A_{HJ,ji}}{\dot{m}_d} \tag{28}$$

Finally, the performance ratio of the desalination system (PR) – defined as the ratio of the mass flow rate of produced fresh water to that of the consumed steam – can be determined as follows:

$$PR = \frac{\dot{m}_d}{\dot{m}_s} \tag{29}$$

3.1.4. Electrical and thermal efficiencies

Electrical efficiency of the cogeneration system (η_{elec}) can be defined as follows:

$$\eta_{elec} = \frac{\dot{W}_{net} - \dot{W}_{pumps}}{\dot{m}_f \times LHV_f} \tag{30}$$

where

$$\dot{W}_{net} = \dot{W}_{SOFC,AC} + \dot{W}_G \tag{31}$$

$$\dot{W}_{SOFC,AC} = \eta_{inverter} \times \dot{W}_{SOFC,DC} \tag{32}$$

$$\dot{W}_G = \eta_G \times \dot{W}_{PT} \tag{33}$$

Furthermore, the first law efficiency of the power generation and HRSG system (η_I) can be expressed by:

$$\eta_I = \frac{\dot{W}_{net} - \dot{W}_{pumps} + \dot{Q}_{HRSG}}{\dot{m}_f \times LHV_f} \tag{34}$$

3.2. Exergy analysis

Exergy is defined as the maximum work that can be obtained from a given system state to environment conditions. The idea behind using an exergy analysis is that it enables designers to find the cause and true magnitude of wastes in the system [46].

Applying the first and second laws of thermodynamics, the steady state exergy balance equation for a general control volume can be expressed as follows:

$$\frac{dE_{cv}}{dt} = \sum_j \dot{E}_j^{\,Q} - \dot{E}^{\,W} + \sum_i \dot{E}_i - \sum_e \dot{E}_e - \dot{E}_D = 0 \tag{35}$$

where $\dot{E}_i$ and $\dot{E}_e$ are the exergy transfer rate at control volume inlets and outlets, $\dot{E}_D$ is the exergy destruction rate due to irreversibilities. $\dot{E}^{\,W}$ is the rate of exergy transfer by work, and $\dot{E}^{\,Q}$ is the rate of exergy transfer by heat transfer, respectively.

Assuming no electromagnetic, electric, nuclear, and surface tension effects, the exergy flow rate of the system can divided into two (separate) parts—physical and chemical exergy [47,48]:

$$\dot{E} = \dot{E}^{\,PH} + \dot{E}^{\,CH} \tag{36}$$

The relations required for calculating the physical exergy of incompressible fluids and ideal gases and also chemical exergy of gaseous mixtures are given in the previous paper of the co-authors [41].

In order to calculate the exergy of seawater, validated specific enthalpy and entropy seawater properties are used—as given by the following empirical curve fits [31]:

$$h_{sw}(T,X) = h_w(T) - X\left[a_1 + a_2X + a_3X^2 + a_4X^3 + a_5T + a_6T^2 + a_7T^3 + a_8XT + a_9X^2T + a_{10}XT^2\right] \tag{37}$$

$$s_{sw}(T,X) = s_w(T) - X\left[b_1 + b_2X + b_3X^2 + b_4X^3 + b_5T + b_6T^2 + b_7T^3 + b_8XT + b_9X^2T + b_{10}XT^2\right] \tag{38}$$

where h_w and s_w are the specific enthalpy and entropy of water, while X is the salinity of seawater (in terms of kg/kg). The constant values in Eqs. (37) and (38) can be found in Ref. [31].

3.2.1. Exergy destruction rate

By applying the exergy balance equation (Eq. (35)) for each system component, the exergy destruction rate of each component is obtained. It should be mentioned that the corresponding equation for the exergy destruction rate of each component in SOFC–GT cycle (including compressors, SOFC stack, combustion chamber, gas turbine, power turbine, recuperators, and water pump) were also presented in detail in our previous paper [41].

The exergy destruction rate of HRSG and MSF desalination system is determined as follows:

$$\dot{E}_{D,HRSG} = \left(\dot{E}_{13} + \dot{E}_{16,i}\right) - \left(\dot{E}_{14} + \dot{E}_{17,o}\right) \tag{39}$$

$$\dot{E}_{D,MSF} = \left(\dot{E}_{17,o} + \dot{E}_{18}\right) - \left(\dot{E}_{16,i} + \dot{E}_{21} + \dot{E}_{22} + \dot{E}_{23}\right) + \dot{W}_{pumps} \tag{40}$$

Though, it should be pointed out that the concentrated brine leaving the MSF unit, from practical point of view, is usually disposed without being utilized and consequently will not have an exergetic value [49–51].

3.2.2. Exergetic efficiency

The exergetic efficiency of the power generation cycle with HRSG can be defined by:

$$\psi_{SOFC\text{-}GT} = \frac{\dot{W}_{net} + \left(\dot{E}_{17,o} - \dot{E}_{16,i}\right)}{\dot{m}_f e_f^{CH}} = 1 - \left(\frac{\dot{E}_{D,SOFC\text{-}GT}}{\dot{m}_f e_f^{CH}}\right) \tag{41}$$

where $\dot{E}_{D,SOFC\text{-}GT}$ is the sum of exergy destruction rate of components in the SOFC–GT–HRSG cycle, and e_f^{CH} is the specific chemical exergy of the fuel (natural gas).

The exergetic efficiency of the MSF desalination system can be expressed as:

$$\psi_{MSF} = \frac{\dot{E}_{21} + \dot{E}_{22} + \dot{E}_{23} - \dot{E}_{18}}{\left(\dot{E}_{17,o} - \dot{E}_{15}\right) + \dot{W}_{pumps}} = 1 - \left[\frac{\dot{E}_{D,MSF}}{\left(\dot{E}_{17,o} - \dot{E}_{15}\right) + \dot{W}_{pumps}}\right] \quad (42)$$

The total exergetic efficiency of the cogeneration system is calculated as:

$$\psi_{tot} = \frac{\dot{E}_{out}}{\dot{E}_{in}} = \frac{\dot{E}_{21} + \dot{E}_{22} + \dot{E}_{23} - \dot{E}_{18} + \dot{W}_{net} - \dot{W}_{pumps}}{\dot{m}_f e_f^{CH}} = 1 - \left(\frac{\dot{E}_{D,tot}}{\dot{m}_f e_f^{CH}}\right) \quad (43)$$

where $\dot{E}_{D,tot}$ is the sum of exergy destruction rate of all the system components in the cogeneration system.

3.3. Economic analysis

In the present work, the economic analysis takes into account both the capital and maintenance costs of the system components and the operational cost of the plant, which includes the cost of fuel consumption.

3.3.1. Capital, maintenance, and operational costs

The considered cost functions for all components are given in Table 1 [32,48,51–55]. The capital cost of each component (Z_k) is accordingly determined and the corresponding cost per unit of time ($\dot{Z}_k$) is determined using the following relation:

$$\dot{Z}_k = \frac{Z_k \times CRF \times \Phi}{N \times 3600} \quad (44)$$

where N is the annual operational hours of the system, Φ is the maintenance factor, and CRF is the capital recovery factor which is obtained based on the considered interest rate, and life time of the system [48].

Table 1
The cost functions in terms of thermodynamic parameters for the system components [32,48,52–55].

System component	Capital cost function
Air compressor	$Z_{AC} = \frac{39.5 \times \dot{m}_a}{0.9 - \eta_{ac}} \left(\frac{p_{dc}}{p_{suc}}\right) \ln\left(\frac{p_{dc}}{p_{suc}}\right)$
Fuel compressor	$Z_{FC} = 91562 \left(\frac{\dot{W}_{FC}}{445}\right)^{0.67}$
Combustion chamber	$Z_{CC} = \left(\frac{46.08 \dot{m}_7}{0.995 - \frac{p_9}{p_7}}\right)[1 + \exp(0.018T_9 - 26.4)]$
Turbine	$Z_T = W_T[1318.5\text{-}98.328\ln(W_T)]$
Generator	$Z_{generator} = 26.18(W_{PT})^{0.95}$
Recuperator	$Z_{REC} = 2290(A_{REC})^{0.6}$
SOFC stack	$Z_{SOFC} = A_{SOFC}(2.96T_{SOFC} - 1907)$
Inverter	$Z_{inverter} = 10^5 \left(\frac{\dot{W}_{SOFC,DC}}{500}\right)^{0.7}$
Auxiliary devices	$Z_{SOFC,aux} = 0.1(Z_{SOFC})$
Pump	$Z_{pump} = 705.48 \times \dot{W}_{pump}^{0.71} \left(1 + \frac{0.2}{1 - \eta_{pump}}\right)$
HRSG	$Z_{HRSG} = 6570\left[\left(\frac{\dot{Q}_{ec}}{\Delta T_{LMTD,ec}}\right)^{0.8} + \left(\frac{\dot{Q}_{ev}}{\Delta T_{LMTD,ev}}\right)^{0.8}\right] + 21276\dot{m}_w + 1184.4\dot{m}^{1.2}{}_g$
Brine heater	$Z_{BH} = 430 \times 0.367 \times \dot{Q}_{BH} \times TTD_{BH}{}^{-0.7} \times \Delta p_t{}^{-0.08} \times \Delta p_s{}^{-0.04}$
HR/HJ section	$Z_{HR/HJ} = 430 \times 1.6 \times \dot{Q}_{HR/HJ} \times \Delta T_n{}^{-0.75} \times TTD_C{}^{-0.5} \times \Delta p_t{}^{-0.1}$

Furthermore, the cost rate corresponding to the fuel cost based on the unit cost of fuel (c_f) can be determined as:

$$\dot{C}_f = c_f \times \left(\frac{LHV}{1000}\right) \times \dot{m}_f \quad (45)$$

3.3.2. The payback period

The payback period is the time required for recovering the capital investment in a plant by selling the output of the system [48]. The worth of a plant's investment in the pth year of operation ($E_{C,p}$) based on the corresponding capital and operation costs can be determined as:

$$E_{C,p} = \left(\sum_k Z_k\right)(1+i)^p + \sum_{m=1}^{p} \dot{C}_f \times N \times 3600\,(1+i)^{p-m} \quad (46)$$

The value of the net income received from selling the generated electricity and distillate fresh water in the pth year is calculated as:

$$E_p = \sum_{m=1}^{p}\left(\dot{W}_{net} - \dot{W}_{pumps}\right) \times N \times c_{elec}(1+i)^{p-m} + \sum_{m=1}^{p} \dot{m}_d \times \frac{1}{\rho_w} \times N \times 3600 \times c_w(1+i)^{p-m} \quad (47)$$

where c_{elec} and c_w are the unit cost of electricity and the distillate product, respectively. Hence, taking into account the aforementioned equations and employing the Newton–Raphson method, the payback period of the plant (p) is obtained.

3.4. Environmental analysis

Increasing environmental concerns necessitates considering the environmental impacts while designing energy systems. Therefore, in the present study, the penalty costs of pollutant emissions are taken into account in the total cost rate of the plant. Carbon monoxide (CO), nitrogen oxides (NO_x), and carbon dioxide (CO_2) are considered as the main emitted pollutants. Since experimental data reveals that the amounts of CO and NO_x generated in SOFC stack is negligible [56], the entire CO and NO_x emission is assumed to take place in the combustion chamber.

Accordingly, the amounts of emitted CO and NO_x, based on the residence time in the combustion zone, τ, and the primary zone combustion temperature, T_{pz}, can be calculated by [57]:

$$m_{CO} = \frac{0.179 \times 10^9 \times \exp\left(\frac{7800}{T_{pz}}\right)}{p^2 \tau \left(\frac{\Delta p}{p}\right)^{0.5}} \quad (48)$$

$$m_{NO_x} = \frac{0.15 \times 10^{16} \times \tau^{0.5} \exp\left(\frac{-71100}{T_{pz}}\right)}{p^{0.05}\left(\frac{\Delta p}{p}\right)^{0.5}} \quad (49)$$

where the emission amounts are given in terms of grams of pollutant per kg of fuel, and $\frac{\Delta p}{p}$ indicates the non-dimensional pressure drop in the combustion chamber. Details for calculation of the τ and T_{pz} are presented in [57,58]. It should be noted that the amount of CO_2 released into the atmosphere can be determined based on the combustion equation in the combustion chamber.

4. System optimization

4.1. Definition of the objective functions

In the present work, the exergetic efficiency and the total cost rate of the aforementioned system are the two objective functions used for the multi-objective optimization procedure. The mentioned objective functions can be expressed using the following relations:

Exergetic efficiency (objective function I)

$$\psi_{tot} = \frac{\dot{E}_{out}}{\dot{E}_{in}} = \frac{\dot{E}_{21} + \dot{E}_{22} + \dot{E}_{23} - \dot{E}_{18} + \dot{W}_{net} - \dot{W}_{pumps}}{\dot{m}_f e_f^{CH}} = 1 - \left(\frac{\dot{E}_{D,tot}}{\dot{m}_f e_f^{CH}}\right) \quad (50)$$

Total cost rate (objective function II)

$$\dot{C}_{tot} = \sum_k \dot{Z}_k + \dot{C}_f + \dot{C}_{env} \quad (51)$$

where

$$\dot{C}_{env} = c_{CO}\dot{m}_{CO} + c_{NO_x}\dot{m}_{NO_x} + c_{CO_2}\dot{m}_{CO_2} \quad (52)$$

In Eq. (52), $\dot{m}_{NO_x}$, $\dot{m}_{CO}$, and $\dot{m}_{CO_2}$ are the exhaust mass flow rates of nitrogen oxides, carbon monoxide, and carbon dioxide, respectively. The terms c_{NO_x}, c_{CO}, and c_{CO_2} are their corresponding damage unit costs.

4.2. Design parameters and constraints

The following design parameters were chosen for optimization of the cogeneration system: the air compressor pressure ratio ($r_{p,AC}$), the isentropic efficiencies of air compressor (η_{AC}), the power turbine (η_{PT}), and the gas turbine (η_{GT}), current density of SOFC stack (i), utilization factors of fuel (U_f) and air (U_a), steam to carbon ratio (S/C), pinch point temperature difference (ΔT_{pp}), motive steam inlet temperature (T_s), number of desalination stages (n), brine temperature in the last stage (T_n), and top brine temperature (TBT).

The aforementioned design parameters and their range of variation as well as the system constraints are listed in Table 2.

4.3. Optimization method

4.3.1. Multi-objective optimization

Most engineering problems deal with number of different and often conflicting objectives which should be satisfied simultaneously. In contrast to a single-objective optimization algorithm, a multi-objective optimization problem does not necessarily produce a unique optimal solution. To achieve the optimal solution, there are trade-offs between objectives. In these types of problems, the interaction of multiple objectives results in a set of non-dominated solutions, called the Pareto front, which provides a decision-maker more flexibility to choose a suitable alternative. There are numerous methods to carry out multi-objective optimization and achieve the set of optimal solutions. Evolutionary algorithms, are naturally suited for these types of problems, and have been widely used for dealing with multi-objective optimization. Accordingly, in this article a multi-objective genetic algorithm (MOGA) has been utilized in order to achieve the optimal solutions.

4.3.2. Genetic algorithm

Genetic algorithm (GA) is a heuristic numerical search algorithm motivated by biological evolution—first presented by Holland [59]. Detailed discussions about gas are given in Refs. [59] and [60]. Being a heuristic algorithm, the main advantage of a GA in comparison with

Table 2
List of constraints for system optimization and their range of variation.

Constraints	Reason
$2 < r_{p,AC} < 16$	For typical, commercially available technology
$0.6 < \eta_{AC} < 0.9$	For typical, commercially available technology
$0.6 < \eta_{GT} < 0.9$	For typical, commercially available technology
$0.6 < \eta_{PT} < 0.9$	For typical, commercially available technology
$1000 < i < 5000$	Minimum and maximum values of cell current density
$0.5 < U_f < 0.9$	Minimum and maximum values of fuel utilization factor
$0.1 < U_a < 0.7$	Minimum and maximum values of air utilization factor
$2 < S/C < 4$	Minimum and maximum values of steam to carbon ratio
$10 < \Delta T_{pp} < 25$	Minimum and maximum values of pinch point temperature difference
$85 < T_s < 125$	Minimum and maximum values of inlet motive steam temperature
$15 < n < 30$	Minimum and maximum values of number of desalination stages
$30 < T_n < 50$	Minimum and maximum values of brine temperature in the last stage
$80 < TBT < 110$	Minimum and maximum values of top brine temperature
$TIT < 1550$ K	Material temperature limit
$T_{SOFC} < 1400$ K	Material temperature limit
$T_{11} > T_{12}$	For driving heat exchange between hot and cold streams in REC 1
$T_{11} > T_3$	For driving heat exchange between hot and cold streams in REC 1
$T_{12} > T_2$	For driving heat exchange between hot and cold streams in REC 1
$T_{12} > T_6$	For driving heat exchange between hot and cold streams in REC 2
$T_{13} > T_5$	For driving heat exchange between hot and cold streams in REC 2
$T_{14} > 400$ K	To avoid formation of sulfuric acid in exhaust gases
$T_{13} > T_{16}$	For driving heat exchange between hot and cold streams in HRSG
$T_{14p} > T_{16} + \Delta T_{pp}$	For driving heat exchange between hot and cold streams in HRSG
$V_v < 8$	The maximum allowable vapor velocity
$H_b < 0.5$	The maximum allowable brine pool height
$2 < \Delta T_{stage} < 4$	Typical range of temperature difference between stages
$X_b \leq 70{,}000$ ppm	Environmental limit

Table 3
Input parameters used for simulation of the cogeneration system.

Parameter	Value
Gas turbine cycle	
Fuel compressor isentropic efficiency (η_{FC})	0.82
Recuperator effectiveness (ε)	0.88
Combustion chamber efficiency (η_{CC})	0.98
Electric generator efficiency (η_G)	0.95
Pump efficiency (η_{pump})	0.83
Solid oxide fuel cell	
DC–AC inverter efficiency ($\eta_{inverter}$)	0.95
SOFC heat loss (percent of MW_{DC}) [56]	1.7
Heat recovery steam generator	
Inlet HRSG water temperature (K)	298
Approach point temperature difference (K)	15
Multi stage flash desalination system	
Intake seawater temperature (K)	303
Intake seawater salt concentration (ppm)	42,000
Rejected brine salt concentration (ppm)	70,000
Outside/inside diameters of the heat recovery condenser tubes (m)	0.0349/0.0316
Outside/inside diameters of the heat rejection condenser tubes (m)	0.0285/0.0253
Number of heat rejection stages (j)	3
Pressure losses	
Recuperator (%)	4
Fuel cell stack (%)	4
Combustion chamber (%)	5
Desulfurizer (%)	3
Fuel (natural gas) properties [46]	
Composition (percent by volume)	CH_4 (95%), C_2H_6 (2.5%), CO_2 (1%), N_2 (1.5%), sulfur compounds (5 ppm_v)
LHV (kJ/kg)	45,100
Specific chemical exergy(kJ/kg)	46,713
Molar weight (kg/kmol)	16.85
Air properties [46]	
Composition (percent by volume)	N_2 (79%), O_2 (21%)
Molar weight (kg/kmol)	28.97

Table 4
Comparison of the computed values of system performance parameters obtained from modeling the MSF desalination system with the values reported in Ref. [69].

Parameter	Unit	Modeling	Reported	Difference (%)
Thermal performance ratio (PR)	–	6.63	6.7	1.04
Specific heat transfer area (sA_{MSF})	$m^2/(kg/s)$	303.4	306.2	0.91
Cooling seawater mass flow rate ($\dot{m}_{CW}$)	kg/s	5.61	5.55	1.08

al gradient based methods, is its capability of evading the local optimums and its ability to handle highly non-linear, complex systems.

In genetic algorithm terminology, a solution vector, **x**, belonging to the set of solutions is called an individual or a chromosome. Chromosomes are constructed from discrete units called genes, each of which controls one or more features of the chromosome [61–63]. A group of chromosomes is called population.

In a GA optimization, three different functions including selection, crossover and mutation are employed. In a population, the individuals are chosen based on their fitness. A higher fitness individual has a higher chance of being chosen for reproduction. In a crossover operator, two chromosomes, which are called parents, are combined in order to produce new chromosomes, called offspring. Due to the fact that individuals with higher fitness have more possibility for being selected and to produce offspring, the new population will obtain better genes and consequently a higher fitness. Therefore, employing a crossover operator in numerous iterations results in convergence to an optimal solution. The mutation function, which is an operator applied at the genes level, generates random changes in properties of chromosomes. Since the mutation rate is low and depends on the length of the chromosome, mutated chromosomes will not be much different from the preceding ones. Hence, crossover enhances convergence by making the chromosomes in the population similar, while the mutation operator reintroduces genetic diversity in the population and assists to evade the local optima [63]. In the present work, the multi-objective GA in MATLAB® optimization toolbox has been used to optimize the objective functions presented in Eqs. (50) and (51). The tuning parameters chosen for our genetic algorithm optimization procedure are tabulated in Table 5.

5. Case study

The aforementioned modeling and optimization approach are applied to find optimal designs for an IRSOFC–GT hybrid cycle coupled to an MSF desalination system with brine recirculation. This system is proposed to be installed in Bandar Abbas, a coastal city in the south of Iran, which has faced an acute shortage of fresh water recently. The required power output of the plant is 2 MW and a heat recovery steam generator is utilized to produce the required motive steam for the MSF desalination unit via recovering the extra heat of the flue gas. The input parameters listed in Table 3 are taken into consideration for simulation of the cogeneration system. Fig. 3 illustrates the profile of the minimum and maximum ambient temperatures over a year in Bandar Abbas [64]. It should be noted that considering the fact that the water experiences negligible fluctuations, a constant sea water temperature has been considered in the present study.

Table 5
Tuning parameters in the optimization program.

Tuning parameters	Value
Population size	300
Maximum number of generations	200
Minimum function tolerance	10^{-5}
Probability of crossover	90%
Probability of mutation	1%
Number of crossover point	2
Selection process	Tournament
Tournament size	2

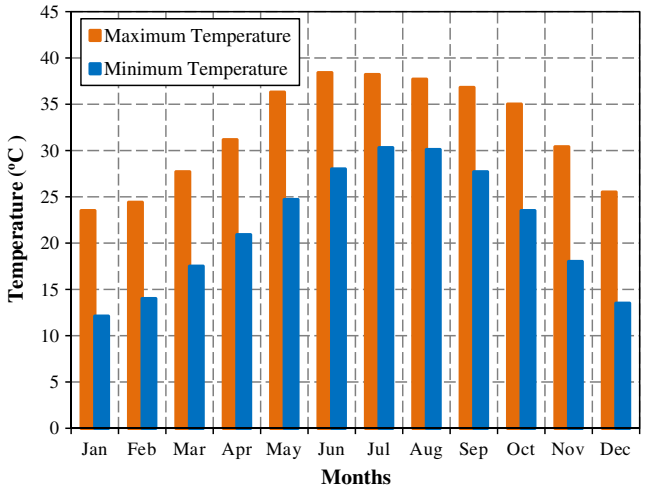

Fig. 3. Ambient temperature variations in Bandar Abbas, Iran, over a year [64].

Working fluid properties are derived from the JANAF Thermodynamic Tables [65].

The corresponding unit costs of generated electricity (c_{elec}), distillate product (c_w), and the fuel (c_f) are considered to be 0.06 USD/kWh, 1.56 USD/m^3, and 0.004 USD/MJ (0.12 USD/m^3), respectively [41,42]. Moreover, the unit damage costs associated with CO (c_{co}), NO_x(c_{NO_x}), and CO_2 (c_{CO_2}) are considered to be 0.02086 USD/kg CO, 6.853 USD/kg NO_x, and 0.0224 USD/kg CO_2, respectively [66,67].

To determine the CRF, the lifetime of the plant (n), the maintenance factor (Φ), and the annual interest rate (i) are considered to be 15 years, 1.06, and 14% [68], respectively. The operational hours per year of the cogeneration system (N) is assumed to be 8040 h.

6. Results and discussion

6.1. Model verification

Details about verification of the IRSOFC–GT hybrid cycle were presented in detail in the previous paper of co-authors [41]. In order to validate the developed model for the desalination system, the main performance parameters of the MSF system – including the thermal performance ratio (PR), the specific heat transfer area (sA_{MSF}), and the cooling seawater mass flow rate ($\dot{m}_{CW}$) – obtained from the developed model are compared with the corresponding values given in Ref. [69]. As shown in Table 4, the mean difference was less than 1.1%, which verifies sufficient accuracy of the developed simulation code to model the thermal performance of the MSF desalination system.

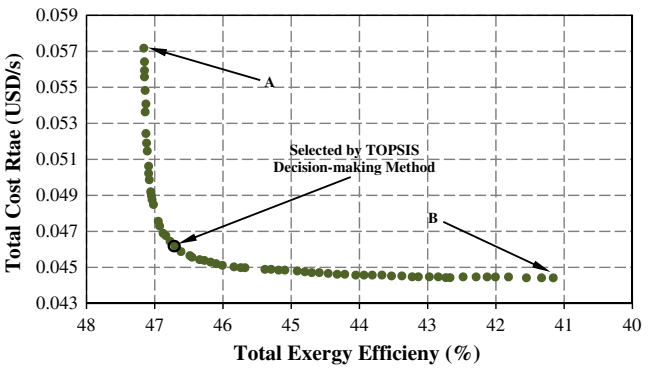

Fig. 4. Pareto optimal frontier obtained from multi-objective optimization of the cogeneration system.

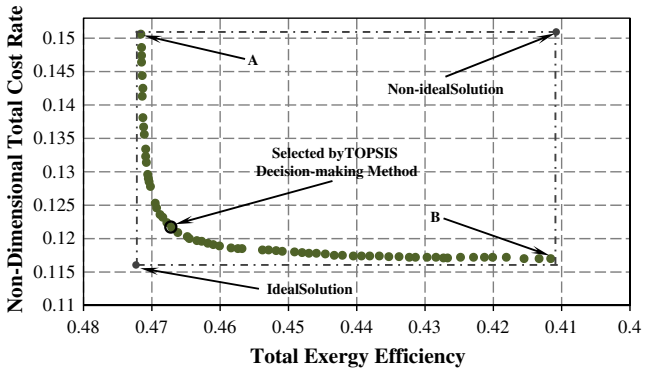

Fig. 5. The set of non-dimensional Pareto optimal solutions using TOPSIS decision-making method to specify the final optimal design point of the cogeneration system.

6.2. Optimization results

By applying the multi-objective optimization procedure, the Pareto optimal solutions – presented in Fig. 4 – is achieved. The previously mentioned conflict between the considered objective functions is evident in this diagram. Each point on the Pareto curve in Fig. 4 shows the possible optimal solutions which satisfy the objectives at an acceptable level without being dominated by any other solution. Among the designs which can result in a specific exergetic efficiency, the chosen point in the Pareto front is the one leading to the lowest possible total cost rate. That is, for any specific total cost rate, the chosen point of Pareto front demonstrates the design with the highest possible exergetic efficiency. Fig. 4 shows that although it is possible to increase exergetic efficiency of the system up to about 44%, this leads to increases in the total cost rate. For example, raising it from 44% to 46.5% results in a moderate increment in the cost rate, but increasing to values higher than 46.5% leads to a severe increase in the total cost rate of the plant. Thus, optimizing the system by only considering the exergetic efficiency as the objective function, leads to the selection of design point A with the highest exergetic efficiency (47.16%) in which has the highest total cost rate (0.05717 USD/s). In contrast, taking into account the

Table 6
The optimal values of system design parameters obtained from the three methods of optimization.

Design parameters	Exergetic optimization (objective function I)	Economic optimization (objective function II)	Multi-objective optimization (objective functions I and II)
$r_{p,AC}$	9.7	7.7	9.1
η_{AC} (%)	88.1	81.1	84.7
η_{GT} (%)	86.3	79.1	83.8
η_{PT} (%)	88.9	81.9	85.6
i (A/m^2)	2491.3	2820.4	2681.7
U_f	0.85	0.78	0.81
U_a	0.30	0.23	0.26
S/C	2.39	2.63	2.48
ΔT_{pp} (K)	18.6	23.9	20.3
T_s (°C)	119.3	112.7	116.1
n	27	21	24
T_n	42.4	44.6	43.3
TBT	102.1	108.6	105.6

Table 7
Stream data of the cogeneration plant at the final optimal design point derived from the TOPSIS decision-making method.

Stream	Pressure (bar)	Temperature (K)	Mass flow rate (kg/s)	Specific exergy (kJ/kg)	Exergy flow rate (kW)
1	1	299.15	1.3624	0	0
2	9.1	611.01	1.3624	293.99	400.54
3	8.74	1000.73	1.3624	565.4	770.31
4	1	299.15	0.0693	0	0
5	9.1	546.06	0.0693	551.81	38.24
6	8.46	731.538	0.0693	48,886	3387.8
7	8.39	1197.73	1.1449	760.28	870.44
8	8.12	1197.73	0.3834	3983.57	1527.32
9	7.84	1424.5	1.5277	1059.5	1618.6
10	4.75	1275.96	1.5277	914.58	1397.2
11	1.93	1091.56	1.5277	623.87	953.1
12	1.85	819.61	1.5277	343.92	525.41
13	1.78	798.35	1.5277	321.29	490.84
14	1.71	402.61	1.5277	67.19	102.64
15	1.68	363.59	0.3364	25.42	8.55
16,i	1.84	363.59	0.3364	25.42	8.55
17,o	1.75	389.25	0.3364	560.11	188.42
18	1	303	13.39	0	0
19	2.35	303	13.39	0	0
20	0.11	314.2	2.96	0.845	2.5
21	1	307.4	2.96	0.845	2.5
22	0.11	316.45	4.4	1.12	4.91
23	1.65	316.45	5.99	1.15	6.9

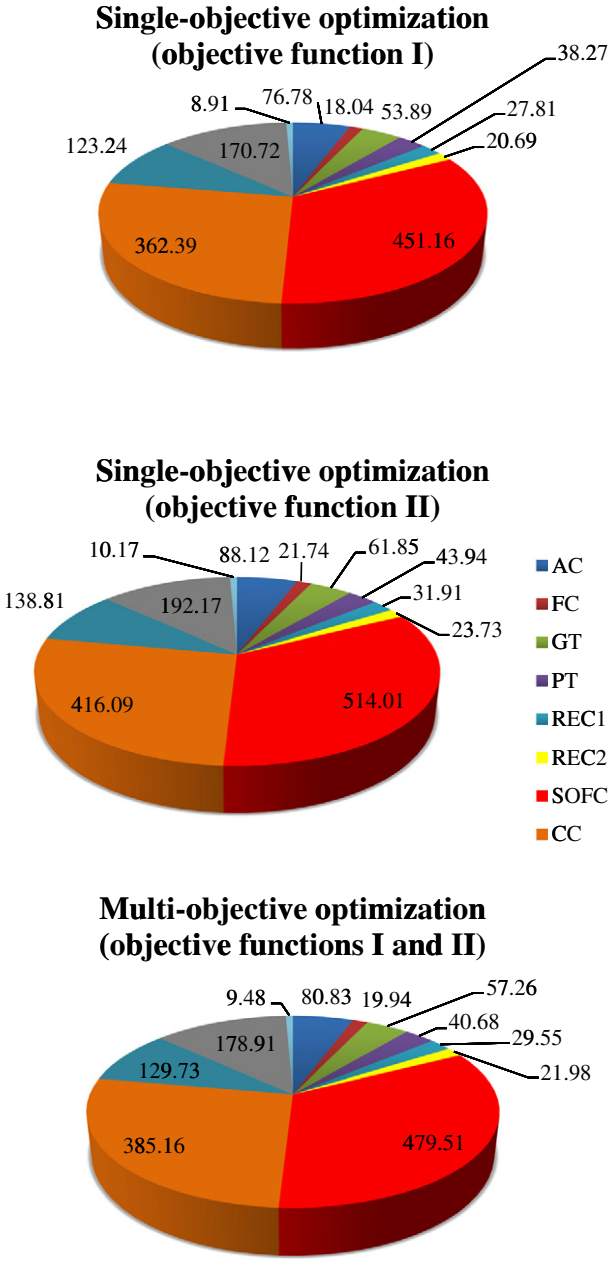

Fig. 6. Exergy destruction rate in various components of the cogeneration system (in terms of kW) at optimal points obtained from three methods of optimization.

Table 8
Capital costs (in terms of MUSD) of various components in cogeneration system at optimal points obtained from the three methods of optimization.

Component	Exergetic optimization (objective function I)	Economic optimization (objective function II)	Multi-objective optimization (objective functions I and II)
AC	0.0214	0.0171	0.0185
FC	0.0199	0.0161	0.0173
GT	0.3556	0.2860	0.3011
PT	0.3974	0.3121	0.3286
REC 1	0.0011	0.00090	0.00095
REC 2	0.000296	0.000230	0.000243
SOFC stack	2.0128	1.5679	1.6507
CC	0.0055	0.0044	0.0046
Inverter	0.3225	0.2641	0.2779
Generator	0.0099	0.0082	0.0087
Auxiliary	0.2013	0.1568	0.1651
HRSG	0.0464	0.0411	0.0442
MSF	0.3957	0.3620	0.3733
Pumps	0.0246	0. 0216	0. 0235

total cost rate as the only objective function, design point B might be selected which leads to the minimum value of the total cost rate (0.04442 USD/s), but also the lowest exergetic efficiency is (41.16%).

As was previously mentioned, all of the achieved points on Pareto front obtained by a multi-objective optimization procedure can be chosen as the optimal design of the system. However, just one optimal design should be chosen. The final optimal point is chosen depending on the priority of each objective for the decision-maker. Numerous approaches for choosing the final optimum design point from the Pareto front are possible. Owing to the fact that the objectives in most of the multi-objective optimization problems have different dimensions (e.g. the total cost rate is expressed in terms of US dollar per unit of time while the exergetic efficiency has no dimension), the values of objective functions should first be non-dimensionalized. The non-dimensionalization method utilized in the present work is the Euclidian technique which was utilized in Ref. [70]. Details of this approach can also be found in Ref. [71]. After applying this method, all the non-dominated optimal solutions are converted to a non-dimensional form.

After applying Euclidian non-dimensionalization, a TOPSIS (Technique for Order Preference by Similarity to an Ideal Solution) decision-making process was employed. In this method, deviation of each solution from the ideal and non-ideal points (illustrated in Fig. 5) is evaluated. The solution with minimum distance from the ideal point and maximum distance from the non-ideal solution is then selected as the final optimal point. The details of this selection algorithm are given in [72,73]. The final optimal design point chosen by TOPSIS decision-making approach, which is demonstrated in Fig. 5, results in the exergetic efficiency of 46.71% with a total cost rate of 0.04619 US/s. Table 6 demonstrates the values of optimal design parameters determined by the single-objective and multi-objective optimization methods. The thermodynamic properties and exergy flow rates of the various streams of the final optimal design point are listed in Table 7.

In order to demonstrate the locations where the exergy losses occur, the exergy destruction rate of each component is given in Fig. 6. These values are obtained at different optimal points achieved by the three methods of optimization including the two single-objectives along with the multi-objective optimization. According to this figure, the highest exergy destruction rate takes place in the SOFC stack (451.16 kW, 514.01 kW and 479.51 kW for the single-objective optimizations considering objective function I and II and multi-objective optimization, respectively). The next highest exergy destruction rates take place at the combustion chamber, the MSF desalination system, HRSG, and the air compressor. It should be pointed out that, as was also previously mentioned, the practical utility of performing the exergy analysis is determining the location and true magnitude of waste due to

Table 9
Performance results of the cogeneration system at optimal points obtained from the three methods of optimization.

Parameter	Exergetic optimization (objective function I)	Economic optimization (objective function II)	Multi-objective optimization (objective functions I and II)
SOFC–GT cycle			
Cell voltage (V)	0.670	0.626	0.659
SOFC temperature (K)	1068.2	1206.3	1149.4
GT inlet temperature (K)	1325.3	1482.6	1424.5
CO_2 emission (kg/year)	5.563×10^6	6.013×10^6	5.658×10^6
CO emission (kg/year)	5.361×10^3	5.897×10^3	5.459×10^3
NO_x emission (kg/year)	133.632	149.555	137.823
Social cost of air pollution (MUSD/year)	0.1256	0.1358	0.1278
Net electrical power output from PT (kW)	394.6	341.2	389.1
Net electrical power output from SOFC (kW)	1740.1	1589.2	1718.3
Waste heat recovery at HRSG (kW)	767.4	692.1	744.5
Exergetic efficiency (%)	58.86	51.29	58.34
MSF system			
Desalination capacity (m^3/day)	274.35	228.66	255.79
Income from selling fresh water (USD/year)	154,074.9	128,415.5	143,651.7
Total steam consumption (kg/s)	0.3378	0.3350	0.3364
Feed seawater (kg/s)	7.94	6.62	7.40
Cooling seawater (kg/s)	6.43	5.58	5.99
Parameter	Single-objective optimization (objective function I)	Single-objective optimization (objective function II)	Multi-objective optimization (objective functions I and II)
Intake seawater (kg/s)	14.37	12.20	13.39
Recycle brine (kg/s)	31.17	24.18	27.84
Blow-down brine (kg/s)	4.76	3.97	4.44
Desalination length (m)	56.712	60.336	58.992
Pumping power consumption (kW)	49.88	41.32	46.53
Specific area (m^2/(kg/s))	308.772	271.182	275.538
Performance ratio	9.4	7.9	8.8
Exergetic efficiency (%)	3.61	3.05	3.49
Electrical efficiency (%)	62.12	53.73	60.73
1st law efficiency of the power generation system (%)	84.11	73.06	82.12
Total exergetic efficiency (%)	47.16	41.16	46.71
Total annual cost (MUSD)	4.5573	3.5858	3.7587

Table 10
Sensitivity analysis of the change in the numerical values of optimal design parameters for the cogeneration system with variations in fuel unit cost.

Change in the values of design parameters	Variation in fuel unit cost			
	−50%	−25%	+25%	+50%
$\frac{\Delta r_{p,AC}}{r_{p,AC}}$	−8.86%	−4.81%	+5.47%	+8.45%
$\frac{\Delta \eta_{AC}}{\eta_{AC}}$	−0.29%	−0.16%	+0.19%	+0.36%
$\frac{\Delta \eta_{GT}}{\eta_{GT}}$	−0.51%	−0.27%	+0.32%	+0.54%
$\frac{\Delta \eta_{PT}}{\eta_{PT}}$	−0.42%	−0.19%	+0.34%	+0.53%
$\frac{\Delta i}{i}$	+5.23%	+2.35%	−3.57%	−6.88%
$\frac{\Delta U_f}{U_f}$	−3.95%	−2.39%	+2.63%	+4.45%
$\frac{\Delta U_a}{U_a}$	−4.29%	−2.20%	+2.45%	+4.22%
$\frac{\Delta(S/C)}{(S/C)}$	+4.66%	+2.29%	−2.43%	−5.04%
$\frac{\Delta(\Delta T_{pp})}{\Delta T_{pp}}$	+9.02%	+5.59%	−4.14%	−8.64%
$\frac{\Delta T_s}{T_s}$	−7.85%	−4.27%	+3.94%	+7.73%
$\frac{\Delta n}{n}$	−8.33%	−4.17%	+4.17%	+8.33%
$\frac{\Delta T_n}{T_n}$	+2.71%	+1.17%	−1.36%	−2.94%
$\frac{\Delta(TBT)}{TBT}$	+6.82%	+3.77%	−3.39%	−6.54%

thermodynamic irreversibilities and inefficiencies. Such information can be useful to show the room for improvement in the plant and to identify the specific components which correspond to the highest amount of loss.

The required capital costs of system components at the obtained optimal points are shown in Table 8. As anticipated, the SOFC stack requires the highest capital investment (2.0128, 1.5679 and 1.6507 MUSD for single-objective I, II, and multi-objective optimization, respectively), while the next highest capital costs can be attributed to the MSF desalination unit, the power turbine, the gas turbine, and the inverter.

Furthermore, the results related to the performance of the cogeneration system at optimal points obtained from aforementioned optimization approaches are indicted in Table 9. By employing the multi-objective procedure, a trade-off between the thermodynamic efficiency and the cost of the system is obtained resulting in an exergetic efficiency of 46.71%.

Furthermore, it should be noted that the magnitude of exergetic efficiency of the MSF plant is quite low, which reveals its high irreversibilities (only 3.61%, 3.05%, and 3.49% for single-objectives I, II, and multi-objective optimization, respectively). This value is very close to the exergetic efficiency presented in Refs. [30,33,74,75] which were found for similar plants.

Additionally, the effect of changing the fuel unit cost on the values of optimal design parameters is reported in Table 10. According to this table, increasing the fuel unit cost makes a shift in the optimal design parameters toward more thermodynamically efficient designs. Moreover, the effect of variation in unit damage cost associated with CO, NO_x, and CO_2 on the total cost and payback period of the system is presented in Table 11. As shown in this table, as the unit damage cost of emissions increases, the total cost and payback period of the system increases, but this rise is not significant due to the fact that SOFCs have low emissions and high capital cost relative to conventional power plants.

Table 11
Optimal values of total cost and payback period of the modeled system under various tariff of unit damage cost of emission.

Variation in unit damage cost	Change in total cost	Change in payback period
−50%	−1.59%	−1.94%
−25%	−0.84%	−1.01%
+25%	+0.87%	+1.03%
+50%	+1.63%	+1.99%

Finally, the payback period of the cogeneration system is estimated to be 8.93 years. Therefore, the initial investment of the installation of the cogeneration plant can be compensated in less than 9 years considering the net income which is received from selling the generated power and distillate fresh water. It should be noted that in spite of the relatively long payback period, SOFC systems have seen a trend of decreasing cost and increasing lifetimes [20]. While this technology is feasible today, it is estimated to be very promising in the near future. It should also be noted that due to the relatively high capital cost of components of the plant (specifically the SOFC stack) most of the plant's benefit is obtained from selling electricity—the fresh water price has a only marginal effect on the payback period of the system.

7. Conclusions

In the present work, an IRSOFC–GT hybrid cycle coupled to an MSF desalination system with brine recirculation was modeled. The modeled system was optimized using a multi-objective genetic algorithm where the total cost rate and exergetic efficiency of the plant were considered as the objectives. A set of optimal values of design parameters of the plant is consequently achieved and a final optimal solution has been chosen, employing a specific selection method. Comparing the results obtained from multi-objective optimization and the optimization procedures considering single function I (the exergetic efficiency) or II (the total cost rate) demonstrated the importance of using multi-objective system optimization in this type of design. The results showed that in the multi-objective optimization, besides preserving high exergetic efficiency, the total cost of the system is also minimized.

Moreover, the optimization results demonstrated that the MSF desalination system is highly irreversible with exergetic efficiency ranging from 3.05 to 3.61% (in all three methods), which dramatically reduces the overall exergetic efficiency of the cogeneration system.

To have a good insight into the modeled cogeneration system performance, a sensitivity analysis was carried out to investigate the effect of variation of fuel unit cost on the achieved optimal design parameters. Finally, it was determined that the initial investment and the associated operational costs are paid back from selling the power output and distillate fresh water in 8.93 years. Despite the relatively long payback period of the proposed configuration, SOFC systems have seen a trend of decreasing cost and increasing lifetimes. Thus, while this technology is feasible today, it is estimated to be very promising in the near future.

Acknowledgments

The authors would like to acknowledge the CRC for Low Carbon Living for providing scholarship support to A. Shirazi.

References

[1] International Energy Oulook, URL: http://www.eia.gov/forecasts/ieo/pdf/0484%282013%29.pdf2013(accessed September 2013).
[2] E. Cardona, A. Piacentino, Optimal design of cogeneration plants for seawater desalination, Desalination 166 (2004) 411–426.
[3] E.M. Ferreira, J.A.P. Balestieri, M.A. Zanardi, Optimization analysis of dual-purpose systems, Desalination 250 (2010) 936–944.
[4] A. Moran, P.J. Mago, L.M. Chamra, Thermoeconomic modeling of micro-CHP (micro-cooling, heating, and power) for small commercial applications, Int. J. Energy Res. 32 (2008) 808–823.
[5] J. Larminie, A. Dicks, Fuel Cell Systems Explained, 2nd ed. John Wiley and Sons Ltd., West Sussex, 2003.
[6] A. Arsalis, Thermoeconomic modeling and parametric study of hybrid SOFC–gas turbine–steam turbine power plants ranging from 1.5 to 10 MWe, J. Power Sources 181 (2008) 313–326.
[7] S.C. Singhal, K. Kendel, High Temperature Solid Oxide Fuel Cell: Fundamental, Design and Applications, Elsevier Ltd., Oxford; New York, 2003.
[8] J. Palsson, A. Selimovic, L. Sjunnesson, Combined solid oxide fuel cell and gas turbine systems for efficient power and heat generation, J. Power Sources 86 (2000) 442–448.
[9] X. Zhang, S.H. Chan, G. Li, H.K. Ho, J. Li, Z. Feng, A review of integration strategies for solid oxide fuel cells, J. Power Sources 195 (2010) 685–702.

[10] G.K. Gupta, J.R. Marda, A.M. Dean, A.M. Colclasure, H. Zhu, R.J. Kee, Performance predictions of a tubular SOFC operating on a partially reformed JP-8 surrogate, J. Power Sources 162 (2006) 553–562.
[11] M. Ni, M.K.H. Leung, D.Y.C. Leung, A modeling study on concentration overpotentials of a reversible solid oxide fuel cell, J. Power Sources 163 (2006) 460–466.
[12] F. Zabihian, A. Fung, A review on modeling of hybrid solid oxide fuel cell systems, Int. J. Eng. 3 (2009) 85–119.
[13] A.V. Akkaya, B. Sahin, H. Huseyin Erdem, An analysis of SOFC/GT CHP system based on exergetic performance criteria, Int. J. Hydrogen Energy 33 (2008) 2566–2577.
[14] J. Wang, Z. Yan, S. Ma, Y. Dai, Thermodynamic analysis of an integrated power generation system driven by solid oxide fuel cell, Int. J. Hydrogen Energy 37 (2012) 2535–2545.
[15] S. Velumani, C. Enrique Guzmán, R. Peniche, R. Vega, Proposal of a hybrid CHP system: SOFC/microturbine/absorption chiller, Int. J. Energy Res. 34 (2010) 1088–1095.
[16] J. Johansen, R.F. Babus'Haq, S.D. Probert, An integrated CHP and desalination plant, Appl. Energy 53 (1996) 157–178.
[17] S.E. Shakib, S.R. Hosseini, M. Amidpour, C. Aghanajafi, Multi-objective optimization of a cogeneration plant for supplying given amount of power and fresh water, Desalination 286 (2012) 225–234.
[18] H.T. El-Dessouky, H.M. Ettouney, Fundamentals of Salt Water Desalination, Elsevier, Amsterdam, 2002.
[19] S. Al-Hallaj, F. Alasfour, S. Parekh, S. Amiruddin, J.R. Selman, H. Ghezel-Ayagh, Conceptual design of a novel hybrid fuel cell/desalination system, Desalination 164 (2004) 19–31.
[20] P. Lisbona, J. Uche, L. Serra, High-temperature fuel cells for fresh water production, Desalination 182 (2005) 471–482.
[21] H.T.A. El-Dessouky, Humidification-dehumidification desalination process using waste heat from a gas turbine, Desalination 71 (1989) 19–33.
[22] M.A. Darwish, N. A1 Najem, Co-generation power desalting plants: new outlook with gas turbines, Desalination 161 (2004) 1–12.
[23] Y. Wang, N. Lior, Performance analysis of combined humidified gas turbine power generation and multi-effect thermal vapor compression desalination systems—Part 1: The desalination unit and its combination with a steam-injected gas turbine power system, Desalination 196 (2006) 84–104.
[24] Y. Wang, N. Lior, Performance analysis of combined humidified gas turbine power generation and multi-effect thermal vapor compression desalination systems: Part 2: The evaporative gas turbine based system and some discussions, Desalination 207 (2007) 243–256.
[25] E. Cardona, A. Piacentino, F. Marchese, Performance evaluation of CHP hybrid seawater desalination plants, Desalination 205 (2007) 1–14.
[26] R. Deng, L. Xie, H. Lin, J. Liu, W. Han, Integration of thermal energy and seawater desalination, Energy 35 (2010) 4368–4374.
[27] D. Maraver, J. Uche, J. Royo, Assessment of high temperature organic Rankine cycle engine for polygeneration with MED desalination: a preliminary approach, Energy Convers. Manag. 53 (2012) 108–117.
[28] S. Motahar, A.A. Alemrajabi, Exergy based performance analysis of a solid oxide fuel cell and steam injected gas turbine hybrid power system, Int. J. Hydrogen Energy 34 (2009) 2396–2407.
[29] M. Hosseini, I. Dincer, P. Ahmadi, H.B. Avval, M. Ziaasharhagh, Thermodynamic modelling of an integrated solid oxide fuel cell and micro gas turbine system for desalination purposes, Int. J. Energy Res. 37 (2013) 426–434.
[30] N. Kahraman, Y.A. Cengel, Exergy analysis of a MSF distillation plant, Energy Convers. Manag. 46 (2005) 2625–2636.
[31] M.A. Al-Weshahi, A. Anderson, G. Tian, Exergy efficiency enhancement of MSF desalination by heat recovery from hot distillate water stages, Appl. Therm. Eng. 53 (2013) 226–233.
[32] D.F. Cheddie, Thermo-economic optimization of an indirectly coupled solid oxide fuel cell/gas turbine hybrid power plant, Int. J. Hydrogen Energy 36 (2011) 1702–1709.
[33] S.R. Hosseini, M. Amidpour, A. Behbahaninia, Thermoeconomic analysis with reliability consideration of a combined power and multi stage flash desalination plant, Desalination 278 (2011) 424–433.
[34] K. Ansari, H. Sayyaadi, M. Amidpour, Thermoeconomic optimization of a hybrid pressurized water reactor (PWR) power plant coupled to a multi effect distillation desalination system with thermo-vapor compressor (MED-TVC), Energy 35 (2010) 1981–1996.
[35] H. Najafi, B. Najafi, Multi-objective optimization of a plate and frame heat exchanger via genetic algorithm, Heat Mass Transf./Waerme- und Stoffuebertragung 46 (2010) 639–647.
[36] H. Najafi, B. Najafi, P. Hoseinpoori, Energy and cost optimization of a plate and fin heat exchanger using genetic algorithm, Appl. Therm. Eng. 31 (2011) 1839–1847.
[37] N. Autissier, F. Palazzi, F. Marechal, J. van Herle, D. Favrat, Thermo-economic optimization of a solid oxide fuel cell, gas turbine hybrid system, ASME J. Fuel Cell Sci. Technol. 4 (2007) 123–129.
[38] F. Palazzi, N. Autissier, F.M.A. Marechal, D. Favrat, A methodology for thermo-economic modeling and optimization of solid oxide fuel cell systems, Appl. Therm. Eng. 27 (2007) 2703–2712.
[39] H. Sayyaadi, M. Babaie, M.R. Farmani, Implementing of the multi-objective particle swarm optimizer and fuzzy decision-maker in exergetic, exergoeconomic and environmental optimization of a benchmark cogeneration system, Energy 36 (2011) 4777–4789.
[40] R.G. Raluy, L. Serra, J. Uche, A. Valero, Life-cycle assessment of desalination technologies integrated with energy production systems, Desalination 167 (2004) 445–458.
[41] A. Shirazi, M. Aminyavari, B. Najafi, F. Rinaldi, M. Razaghi, Thermal–economic–environmental analysis and multi-objective optimization of an internal-reforming solid oxide fuel cell–gas turbine hybrid system, Int. J. Hydrogen Energy 37 (2012) 19111–19124.
[42] S.R. Hosseini, M. Amidpour, S.E. Shakib, Cost optimization of a combined power and water desalination plant with exergetic, environment and reliability consideration, Desalination 285 (2012) 123–130.
[43] S. Sanaye, S. Asgari, Four E analysis and multi-objective optimization of combined cycle power plants integrated with Multi-stage Flash (MSF) desalination unit, Desalination 320 (2013) 105–117.
[44] S.H. Chan, H.K. Ho, Y. Tian, Modelling of simple hybrid solid oxide fuel cell and gas turbine power plant, J. Power Sources 109 (2002) 111–120.
[45] N.F. Bessette II, W.J. Wepfer, Electrochemical and thermal simulation of a solid oxide fuel cell, Chem. Eng. Commun. 147 (1996) 1–15.
[46] T.J. Kotas, The Exergy Method of Thermal Plant Analysis, Krieger Publication Co., Florida, 1995.
[47] S. Sanaye, A. Shirazi, Thermo-economic optimization of an ice thermal energy storage system for air-conditioning applications, Energy Build. 60 (2013) 100–109.
[48] A. Bejan, G. Tsatsaronis, M. Moran, Thermal Design and Optimization, John Wiley and Sons, New York, 1996.
[49] A. Piacentino, F. Cardona, Advanced energetics of a Multiple Effects Evaporation (MEE) desalination plant: Part I: 2nd principle analysis by a zooming representation at single-effect level, Desalination 264 (2010) 84–91.
[50] A. Piacentino, E. Cardona, Advanced energetics of a Multiple-Effects-Evaporation (MEE) desalination plant. Part II: Potential of the cost formation process and prospects for energy saving by process integration, Desalination 259 (2010) 44–52.
[51] K.S. Spiegler, Y.M. El-Sayed, The energetics of desalination processes, Desalination 134 (2001) 109–128.
[52] L. Galanti, A.F. Massardo, Micro gas turbine thermodynamic and economic analysis up to 500 kWe size, Appl. Energy 88 (2011) 4795–4802.
[53] P. Roosen, S. Uhlenbruck, K. Lucas, Pareto optimization of a combined cycle power system as a decision support tool for trading off investment vs. operating costs, Int. J. Therm. Sci. 42 (2003) 553–560.
[54] H. Sayyaadi, Multi-objective approach in thermoenvironomic optimization of a benchmark cogeneration system, Appl. Energy 86 (2009) 867–879.
[55] Y.M. El-Sayed, Designing desalination systems for higher productivity, Desalination 134 (2001) 129–158.
[56] M.C. Williams, Fuel Cell Handbook, 7th ed. EG&G Technical Services, Inc. Science Applications International Corporation, Morgantown, 2004.
[57] N.K. Rizk, H.C. Mongia, Semi analytical correlations for NOx, CO and UHC emissions, J. Eng. Gas Turbines Power 115 (1993) 612–629.
[58] O.L. Gulder, Flame temperature estimation of conventional and future jet fuels, J. Eng. Gas Turbines Power 108 (1986) 376–380.
[59] J.H. Holland, Adaptation in Natural and Artificial Systems, University of Michigan Press, 1975.
[60] D. Goldberg, Genetic Algorithms in Search, Optimization, and Machine Learning, Addison-Wesley Professional, 1989.
[61] T. Selleri, B. Najafi, F. Rinaldi, G. Colombo, Mathematical modeling and multi-objective optimization of a mini-channel heat exchanger via genetic algorithm, J. Therm. Sci. Eng. Appl. 5 (2013).
[62] B. Najafi, H. Najafi, M.D. Idalik, Computational fluid dynamics investigation and multi-objective optimization of an engine air-cooling system using a genetic algorithm, Proc. Inst. Mech. Eng. C J. Mech. Eng. Sci. 225 (2011) 1389–1398.
[63] A. Konak, D.W. Coit, A.E. Smith, Multi-objective optimization using genetic algorithms: a tutorial, Reliab. Eng. Syst. Saf. 91 (2006) 992–1007.
[64] World Weather Information Service, Weather Information for Bandar Abbas, URL: http://www.worldweather.org/114/c00943.htm2012(accessed September 2013).
[65] W. Malcolm, NIST-JANAF Thermodynamic Tables Part 1 and 2, 4th ed. Am. Chem. Soc. Am. Inst. Phys., New York, 1989.
[66] US Department of Energy, Social cost of carbon for regulatory impact analysis under executive order 12866, URL: http://www1.eere.energy.gov/buildings/appliance_standards/residential/pdfs/hvac_app_16-a_social_cost_carbon_2011-04-25.pdf 2012(accessed September 2013).
[67] A. Lazzaretto, A. Toffolo, Energy, economy and environment as objectives in multi-criterion optimization of thermal systems design, Energy 29 (2004) 1139–1157.
[68] Iranian Central Bank, URL: http://www.cbi.ir2011(accessed September 2013).
[69] H. El-Dessouky, I. Alatiqi, H. Ettouney, Process synthesis: the multi-stage flash desalination system, Desalination 115 (1998) 155–179.
[70] M. Navidbakhsh, A. Shirazi, S. Sanaye, Four E analysis and multi-objective optimization of an ice storage system incorporating PCM as the partial cold storage for air-conditioning applications, Appl. Therm. Eng. 58 (2013) 30–41.
[71] H. Sayyaadi, R. Mehrabipour, Efficiency enhancement of a gas turbine cycle using an optimized tubular recuperative heat exchanger, Energy 38 (2012) 362–375.
[72] Z. Yue, A method for group decision-making based on determining weights of decision makers using TOPSIS, Appl. Math. Model. 35 (2011) 1926–1936.
[73] S. Sanaye, A. Shirazi, Four E analysis and multi-objective optimization of an ice thermal energy storage for air-conditioning applications, Int. J. Refrig. 36 (2013) 828–841.
[74] A.S. Nafey, H.E.S. Fath, A.A. Mabrouk, Exergy and thermoeconomic evaluation of MSF process using a new visual package, Desalination 201 (2006) 224–240.
[75] O.A. Hamed, M.A.K. Al-Sofi, M. Imam, G.M. Mustafa, K. Ba Mardouf, H. Al-Washmi, Thermal performance of multi-stage flash distillation plants in Saudi Arabia, Desalination 128 (2000) 281–292.